RSC Advances

ROYAL SOCIETY OF CHEMISTRY

www.rsc.org/advances

Journal Name

ARTICLE TYPE

Cite this: DOI: 10.1039/xxxxxxxxxx

Influence of high energy milling on the microstructure and magnetic properties of the Al-Cu-Fe phases: the case of the *i*-$Al_{64}Cu_{23}Fe_{13}$ quasicrystalline and the ω-$Al_{70}Cu_{20}Fe_{10}$ crystalline phases

Mirtha Pillaca Quispe,*[a‡] Carlos V. Landauro,[a] Milida Z. Pinto Vergara,[a] Justiniano Quispe-Marcatoma,[a] Chachi Rojas-Ayala,[a] Víctor A. Peña-Rodríguez,[a] and Elisa Baggio-Saitovitch[b]

Received Date
Accepted Date

DOI: 10.1039/xxxxxxxxxx

www.rsc.org/journalname

The effect of mechanical milling in *i*-$Al_{64}Cu_{23}Fe_{13}$ quasicrystalline and ω-$Al_{70}Cu_{20}Fe_{10}$ crystalline phases is systematically investigated in the present work. The Al-Cu-Fe samples were obtained by arc furnace technique and then nanostructured by means of mechanical milling. The results indicate that the solid samples present a weak ferromagnetic behavior at 300 K, showing a saturation magnetization of 0.124 emu/g for the icosahedral phase (*i*-phase) and 0.449 emu/g for the tetragonal phase (ω-phase). These small values could be an indication that only a few percentage of Fe atoms carry magnetic moment. The magnetic response in the nanostructured ω-phase increases up to 3.5 times higher than its corresponding solid counterpart. Whereas for the *i*-phase this increment is about 16 times higher. Moreover, the speed of the variation of the studied physical parameters after reducing the average grain size has been obtained from the exponent (α) of a power law fit of the experimental data. The values of α, corresponding to the magnetic response, are slightly different in each phase, which should be related to the different chemical composition and/or the type of long range order. Additionally, we also search for a critical grain size. However, this critical value has not been observed in the studied samples.

1 Introduction

Over the past few decades, major research works have been made in both: understanding and application of quasicrystals (QCs) [1–3], which are aperiodic crystals with long range order but without translational symmetry [4]. However, many questions about their physical properties remain without conclusive and satisfactory answer. In particular, the magnetic properties of these new materials are controversial since they reveal different magnetic responses (diamagnetism [5–7], paramagnetism [8], ferromagnetism [9], and even spin-glass state [10,11]) that are usually associated to many factors such as preparation techniques, impurities, size of particle powder, among others [12]. Many theoretical and experimental works have been performed with the goal of elucidate the origin of these different magnetic behaviors in quasicrystals.

The first studies of magnetism in the stable icosahedral Al-Cu-Fe [13] phase have shown that local atomic environments (i.e., the nearest-neighbors coordination shell of the Fe atoms in *i*-Al-Cu-Fe) play an important role in the magnetic nature of these alloys [8,12]. Thus, these works have indicated the non-magnetic character of the Al-Cu-Fe quasicrystal. Furthermore, a recent work [14] reported that single-quasicrystalline icosahedral $Al_{64}Cu_{23}Fe_{13}$ samples, considered to be in the ideal icosahedral composition, are diamagnetic in the whole temperature range (2 - 300 K) with a Curie-Weiss temperature near to $\theta = -2.3\,K$. Taking into account that the studied sample was a mono-quasicrystal of high structural quality, they considered this behavior as an intrinsic property of the *i*-Al-Cu-Fe quasicrystal. Accordingly, one important conclusion is that the presence of defects, strain, grain size, and grain boundaries may influence the physical properties of the *i*-Al-Cu-Fe QC in such a way that they can overlap the true intrinsic properties of quasicrystals [14].

In particular, the grain boundary volume is a relevant parameter in nanostructured materials (NM). This is because the grain

[a] *Faculty of Physical Sciences, National University of San Marcos, P.O. Box 14-0149, Lima 14, Peru. E-mail: mpillacaq@unmsm.edu.pe*
[b] *Centro Brasileiro de Pesquisas Físicas (CBPF), Rua Dr. Xavier Sigaud 150, Urca, Rio de Janeiro, 22290-180, Brazil*
‡ Present address: Crystallography Section, Department of Earth and Environmental Sciences, Ludwig-Maximilians-Universität München, Theresienstraβe 41, 80333 München, Germany. E-mail: mirtha.pillaca@campus.lmu.de

boundary volume fraction increases after reducing the grain size due to the nanostructuration process. Consequently, grain boundaries growth leads to significant changes in the physical properties of the system under study. However, these effects have been poorly studied. Despite the fact that there are several methods to synthesize NM, among them, mechanical milling (MM) technique has been extensively used for the nanostructuration of materials[15,16]. This is not only due to the low production costs at the industrial level but also for producing NM with a high density of interstitial regions. Thus, MM techniques are a good tool if our purpose is to study the influence of the nanostructuration process on the physical properties of the system. Moreover, it would be interesting to manipulate these properties, in a controlled way, for specific technological applications. In this regard, in a recent work[17] it has been shown that a power law type fit of the simulations can be successfully used to describe the physical properties in function of the size of the system. Another important point to be considered in this adjustment is that these nanostructuration processes also depend on specific characteristics of the system such as: (*i*) periodicity or aperiodicity, and (*ii*) chemical composition. In this sense, the study of both the *i*-$Al_{64}Cu_{23}Fe_{13}$ quasicrystal and its crystalline counterpart ω-$Al_{70}Cu_{20}Fe_{10}$[18] phases are a suitable option to perform such researches.

In the context described above, the present work reports a systematic comparative study of the influence of mechanical milling on the microstructure and magnetic properties of the *i*-$Al_{64}Cu_{23}Fe_{13}$ quasicrystal and the ω-$Al_{70}Cu_{20}Fe_{10}$ crystalline phases. The synthesis and the milling process were performed at least twice to verify the reproducibility of the results. Additionally, the dependence of the physical parameters in function of the average grain is analyzed. The paper is organized as follows. The experimental details are described in the next section. Section 3 is devoted to the results and section 4 to the discussions. Finally, the conclusions are given in section 5.

2 Experimental details

Samples of Al-Cu-Fe alloys, quasicrystalline *i*-$Al_{64}Cu_{23}Fe_{13}$ and crystalline ω-$Al_{70}Cu_{20}Fe_{10}$ phases, have been prepared following previous works[18–20]. First, to obtain the solid sample high-purity elements of Al (99.999%), Fe (99.5%) and Cu (99.9%) were melted in an arc furnace (the ingots were re-melted several times to ensure homogeneity). Subsequently, the solid samples (previously settled in a quartz tube under argon atmosphere) were annealed at 700°C and 600°C to obtain the quasicrystalline and crystalline phase, respectively. Second, in order to obtain nanostructured samples, a mechanical milling process was carried out employing a high energy ball milling equipment (SPEX 8000) with a 7:1 ball-to-powder weight ratio. Solid Al-Cu-Fe samples ($\sim$1.5 g for each milling step) were loaded into a spheric hardened steel vial and mechanically milled for different periods of time up to 5 h using small steel balls of 5 mm diameter. In order to reduce the adherence of the powder to the vial walls and grinding balls we added ethanol during MM. Moreover, the sample manipulation and the containers sealing procedures were performed in a steel box under Ar gas flow in order to prevent powder oxidation. Additionally, the samples preparation procedures (synthesis and nanostructuration) have been repeated twice in order to verify the reproducibility of the experimental results. Hereafter, we will refer to each set of samples as series A and series B.

The obtained products were characterized by different methods and techniques. The phases and the grain size of the samples were analyzed by means of X-ray diffraction (XRD) technique employing a Bruker-D8 Focus diffractometer at 40 kV and 40 mA with Cu-Kα radiation (λ=1.5406 Å). The local structure around the Fe sites was analyzed by a transmission Mössbauer spectrometer (TMS) with a 25 mCi ^{57}Co/Rh radioactive source. Mössbauer spectra were fitted using the NORMOS program[21]. The isomer shift values are given relative to the α-Fe. Finally, the magnetic properties were measured with a vibrating sample magnetometer (VSM) using a Quantum Design equipment with a magnetic field, H, in the range of $\pm$20 kOe. All measurements were recorded at room temperature (RT).

3 Results

3.1 Al-Cu-Fe solid samples

Fig. 1 shows XRD patterns corresponding to heat-treated Al-Cu-Fe samples obtained from the series A. In Fig. 1(a) all diffraction peaks can be indexed as an icosahedral structure identified as *i*-$Al_{64}Cu_{23}Fe_{13}$ phase (*i*-phase). The indexation of each XRD peak of the quasicrystalline phase was made by using the *N/M* indices proposed by Cahn *et al.*[22], which is a short-hand notation of the full 6D indices ($hklh'k'l'$)[22,23]. The narrow shapes and intensities of the diffraction peaks are representative of an icosahedral material of high structural perfection. Also, there is no presence of other crystalline phases such as ε-Al_2Cu_3 and λ-$Al_{13}Fe_4$ found in the as cast sample (see inset of Fig. 1(a)). Similar results have also been observed in the literature[19,24]. In similar way, Fig. 1(b) shows the X-ray diffraction pattern for the heat treated $Al_{70}Cu_{20}Fe_{10}$ alloy. The XRD pattern for the corresponding as cast sample (see inset of Fig. 1(b)) shows a mixture of crystalline phases (θ-Al_2Cu, λ-$Al_{13}Fe_4$, η-AlCu and *fcc*-Al). The weight percent (Wt.%) of each phase found in the as cast $Al_{70}Cu_{20}Fe_{10}$ alloy have already been indicated in a previous work[18]. After heat-treatment, these phases disappear and, consequently, the $Al_{70}Cu_{20}Fe_{10}$ phase (ω-phase) with a small amount of remaining Aluminum *fcc*-phase ($\sim$3.8%Wt.) are formed. This result is according with the Al-Cu-Fe phase diagram where both phases are present. The ω-phase is an ordered tetragonal structure (with space group P4/mnc and lattice parameters: a=6.336(1) Å, c=14.870(2)Å). Based in this information, the corresponding XRD peaks (more than 25 diffraction peaks) has been indexed by Miller indices (*hkl*), in similar way as reported in the literature[25].

3.2 Nanostructured Al-Cu-Fe samples

3.2.1 Structural characterization

X-ray diffraction patterns and Mössbauer spectra of Al-Cu-Fe samples for different milling time intervals, from 0 to 5 h, are shown in Fig. 2. The label 0 h (zero hours milling time) corresponds to the un-milled Al-Cu-Fe (solid) samples, described in more detail in section 3.1. From the XRD patterns of *i*-$Al_{64}Cu_{23}Fe_{13}$, see Fig.

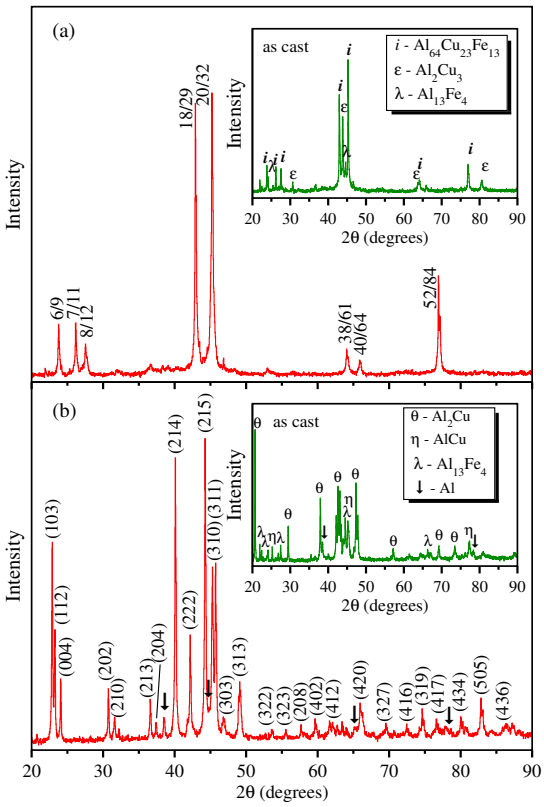

Fig. 1 X-ray diffraction pattern of the Al-Cu-Fe samples obtained after heat treatment at 700 ℃. (a) $Al_{64}Cu_{23}Fe_{13}$ icosahedral quasicrystalline phase, the corresponding N/M (reduced) indices[23] are also indicated. (b) $Al_{70}Cu_{20}Fe_{10}$ tetragonal crystalline phase including the Miller indices (*hkl*), similar as reported in the literature[25]. The insets show their corresponding as cast samples where some metastable crystalline phases (ε-Al_2Cu_3, λ-$Al_{13}Fe_4$, θ-Al_2Cu, η-AlCu and *fcc*-Al) co-exist.

2(a), it is evident the structural stability of the samples under these milling conditions: there is no formation of other phases during the milling process. In similar way, the XRD patterns of the Fig. 2(c), corresponding to the ω-$Al_{70}Cu_{20}Fe_{10}$ sample, show the same behavior for different milling times. Also, the aluminum remaining phase disappears after 1.5 h milling, without producing new XRD peaks (incorporation of Al in the existing phase[26]). Another relevant feature of Figs. 2(a) and 2(c) is a systematic decrease in the intensities and an increment of the corresponding broadenings in the full width at half maximum (FWHM) of the XRD peaks during milling, meaning that the average grain size of the samples become smaller. The estimation of the average grain size of the heat-treated un-milled (solid) and milled (nanostructured) samples were determined from the line broadening of the diffraction peak in the XRD patterns using the Scherrer formula[27],

$$\langle D\rangle = \frac{k\lambda}{\beta\cos\theta}, \qquad (1)$$

where $\langle D\rangle$ is the average grain size, k the shape factor whose value is approximately 0.9, λ is the wavelength of the X-ray radiation (1.5406 Å), β is the pure broadening of the measured diffraction peak (FWHM parameter), and θ the peak position ($2\theta = 42.9°$ for i-phase and $2\theta = 40.2°$ for ω-phase). The contribution of the instrumental width in the diffraction lines was also considered to determine $\langle D\rangle$. The calculated values for the average grain size of Al-Cu-Fe samples as a function of milling time are presented in Fig. 3. As expected, the $\langle D\rangle$ values obtained for both series, A (circles) and B (squares), have the same trend. These results verify the reproducibility of the milling process. Thus, as shown in Fig. 3(a), the grain size evolution during milling for the i-phase is as follow: at the beginning we observe that the MM process leads to a rapid decrease of $\langle D\rangle$ from ∼111 nm (0 h) to ∼27 nm after 1 h. Then, $\langle D\rangle$ decreases slowly up to ∼9 nm after five hours of milling. Analogously, in Fig. 3(b) can be seen a similar behavior for the ω-phase, where the largest changes in the average grain size ocurred during the first hours of milling (from ∼82 nm to 21 nm after one hour milling).

It is worth mentioning that although the Scherrer method is not the best way to calculate $\langle D\rangle$, it can be considered as a good approximation to carry out a systematic study of the effect of the nanostructuration process on the physical properties of the studied samples. Moreover, according to the Rietveld refinement, due to the small value of the lattice strain (∼0.19) produced in the $Al_{70}Cu_{20}Fe_{10}$ phase after five hours milling[18], it is possible to neglect this effect in the present analysis for both kind of samples: the i-phase and the ω-phase.

In order to compare the variation of the average grain size during the MM of both phases we determine the slope of the log-log plot (base 10) of $\langle D\rangle$ versus t (see inset of Fig. 3). Thus, the slope value for the i-phase is -0.59 which is very close to the theoretical value of $-2/3$ (see Ref.[28]), as was also observed in other phases[28]. However, the corresponding slope value for the ω-phase is -0.19, which is very different to the expected theoretical value. This is an indication that the dependence of the mechanical properties on the grain size for both phases are very different.

3.2.2 Microstructural characterization

Fig. 2(b) presents the typical Mössbauer spectra for the quasicrystal (zero hours milling time) and the milled samples, which were fitted considering a quadrupole distribution component and setting the full width at half maximum Γ=0.248 mm/s for all sites[19]. This criterion was also employed in other works[19,29] because the quasicrystalline samples already present intrinsic disorder. The corresponding distributions of the quadrupole splitting, P(Δ), are also shown in the right panels of Fig. 2. Additionally, in order to compare the hyperfine parameters of the ω-phase with the i-phase we used the same criterion to fit the Mössbauer spectra of the ω-phase. The relevant Mössbauer or hyperfine parameters (isomer shift, $\langle\delta\rangle$, and quadrupole splitting, $\langle\Delta\rangle$) obtained from the fit of both Al-Cu-Fe phases are summarized in Table 1. The average isomer shift $\langle\delta\rangle$ and quadrupole splitting $\langle\Delta\rangle$ values fitted for 0 h samples are in good agreement with those reported in the literature[8,20]. Comparing Figs. 2(b) and 2(d) for 0h milling, we can note the differences in the spectra for the i-phase and ω-phase. These results indicate that even at short range the ω-$Al_{70}Cu_{20}Fe_{10}$ phase has different local atomic environment than the i-$Al_{64}Cu_{23}Fe_{13}$. The discussion of these results will be presented in the next section.

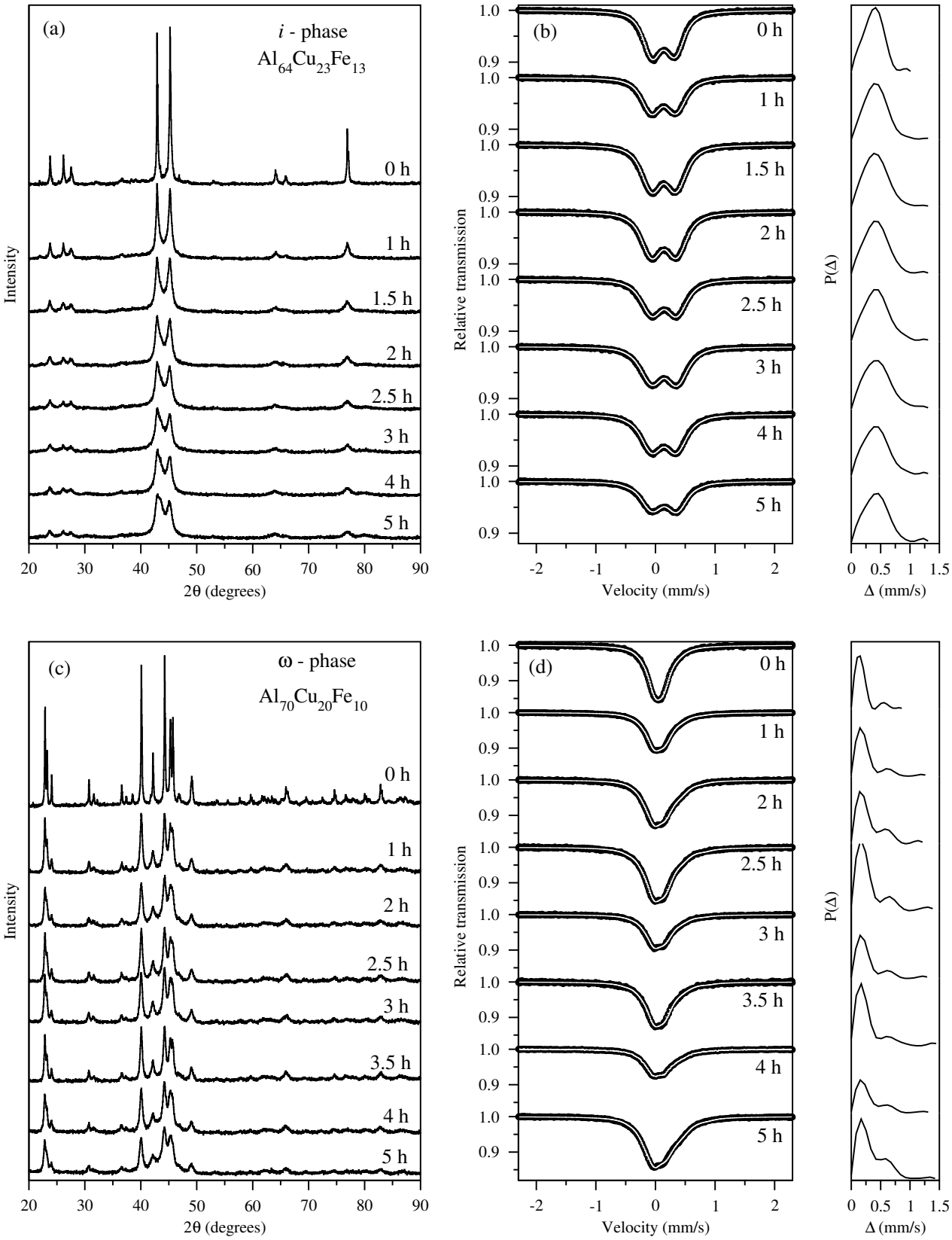

Fig. 2 X-ray diffraction patterns and Mössbauer spectra of Al-Cu-Fe samples for different milling times, as indicated in the figure. (a), (b) correspond to the i-$Al_{64}Cu_{23}Fe_{13}$ quasicrystalline phase, and (c), (d) to the ω-$Al_{70}Cu_{20}Fe_{10}$ crystalline phase. The XRD patterns evidence the high structural stability during the milling process. The typical Mössbauer spectra for both i-$Al_{64}Cu_{23}Fe_{13}$ and ω-$Al_{70}Cu_{20}Fe_{10}$ can be seen in (b) and (d), respectively. The right panels correspond to the quadrupole distributions $P(\Delta)$ for each case of the left.

Table 1 Hyperfine (isomer shift, $\langle\delta\rangle$, quadrupole splitting, $\langle\Delta\rangle$) and magnetic (saturation magnetization, M_s, and coercivity H_c) parameters for the Al-Cu-Fe samples at different milling times. The corresponding average grain size for each phase is also shown. The $\langle\delta\rangle$ values are given relative to the value for α-Fe at room temperature. The values presented here correspond to samples belonging to the series A

Milling	i-$Al_{64}Cu_{23}Fe_{13}$					ω-$Al_{70}Cu_{20}Fe_{10}$				
time	$\langle D\rangle$	$\langle\delta\rangle$	$\langle\Delta\rangle$	M_s	H_c	$\langle D\rangle$	$\langle\delta\rangle$	$\langle\Delta\rangle$	M_s	H_c
(h)	(nm)	(mm/s)	(mm/s)	(emu/g)	(Oe)	(nm)	(mm/s)	(mm/s)	(emu/g)	(Oe)
0.0	110.88(2)	0.241(1)	0.390(1)	0.124(4)	17.41(1))	76(3)	0.170(3)	0.198(2)	0.449(6)	20.12(9)
0.5	41.30(2)	0.244(1)	0.410(1)	0.784(4)	(27.72(6)	28(6)	0.179(6)	0.229(2)	0.854(6)	30.11(5)
1.0	25.92(2)	0.244(1)	0.434(2)	0.727(5)	80.32(7)	21(5)	0.184(7)	0.277(2)	1.063(4)	57.08(9)
1.5	16.76(2)	0.248(0)	0.437(1)	0.969(5)	80.68(4)	—	—	—	—	—
2.0	13.88(2)	0.250(0)	0.440(2)	1.166(4)	94.46(1)	19(2)	0.197(7)	0.317(2)	1.176(6)	78.33(7)
2.5	12.55(2)	0.252(0)	0.454(1)	1.108(4)	111.13(9)	18(3)	0.191(8)	0.317(3)	1.389(4)	49.12(8)
3.0	11.14(2)	0.254(1)	0.464(1)	1.045(4)	127.45(6)	21(5)	0.188(8)	0.294(2)	1.368(5)	74.98(7)
4.0	10.68(2)	0.249(1)	0.457(2)	1.465(4)	81.85(8)	18(1)	0.200(7)	0.324(2)	—	—
5.0	8.40(2)	0.258(1)	0.460(2)	1.994(5)	117.22(9)	17(4)	0.208(8)	0.370(2)	1.602(5)	94.78(2)

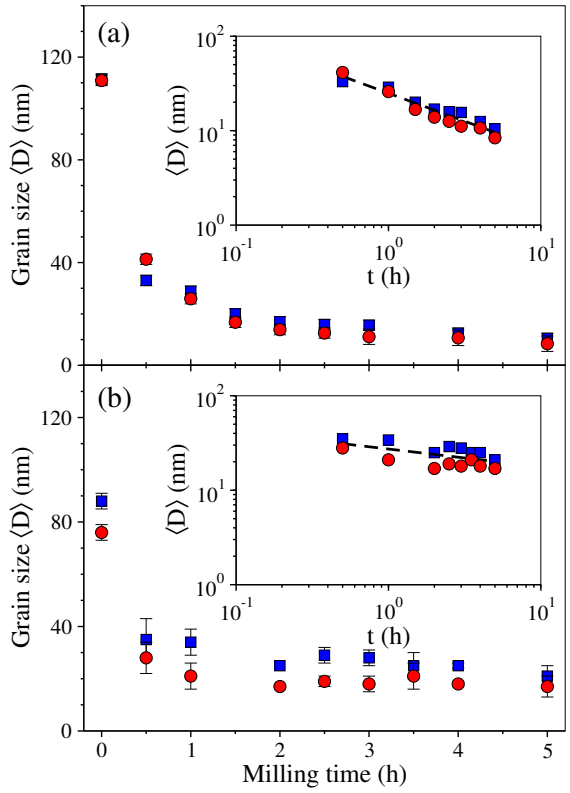

Fig. 3 Evolution of the average grain size $\langle D\rangle$ as function of the milling time for both (a) the i-phase and (b) the ω-phase. (○ series A, □ series B). Inset: log-log plot of $\langle D\rangle$ versus t ($t > 0$). The slopes corresponding to the i-phase and ω-phase (-0.59 and -0.19, respectively) were obtained from a linear fit of the experimental data. The error bars are smaller than or equal to the symbol sizes and correspond to the accuracy determining the line-width of the difraction peaks employed in eqn. (1).

3.2.3 Magnetization measurements

Fig. 4 shows the RT magnetization curves as a function of the external magnetic field, $M(H)$, for the studied samples. From the figure it is clear that the $M(H)$ curves change for all milling times in both phases. It can also be seen that the magnetization curves can not reach a saturation state yet at 20 kOe. For this reason, following Ref.[30], the saturation magnetization was obtained by plotting M vs. $1/H$ and extrapolating the data to infinite field (considering 1/H→0). Moreover, we observe in this figure that the curves for both compositions (i-$Al_{64}Cu_{23}Fe_{13}$ and ω-$Al_{70}Cu_{20}Fe_{10}$) present hysteresis (see insets for a more detailed view), suggesting a ferromagnetic behavior in the initial samples, i.e., zero hours milling. The measured coercive field value after increasing the applied field ($|H_c^+|$) is slightly different to the decreasing one ($|H_c^-|$). It is worth noting that this difference could probably be related to an exchange bias effect (see for instance Ref.[31]). However, in order to quantify the effect of the nanostructuration on the coercive field, we just consider the mean value $H_c = (|H_c^+| + |H_c^-|)/2$.

The magnetic parameters (saturation magnetization, M_s, and coercive field, H_c) are given in Table 1. It can be seen that M_s in the nanostructured ω-$Al_{70}Cu_{20}Fe_{10}$ phase increases up to 3.5 times higher than its corresponding solid counterpart. Surprinsingly, for the case of the i-$Al_{64}Cu_{23}Fe_{13}$ phase this increment is about 16 times. The origin of this behavior will be discussed below.

4 Discussion

According to the XRD patterns shown in the previous section, we observe that the absence of new phases during the milling process is due to the stability of the samples. In fact, recently we reported that even up to 60 hours there is no evidence of the formation of any other phase[32], which is in disagreement with the work of Mukhopadhyay *et al.*[33] and Patiño *et al.*[34] who have shown the structural transformation of the quasicrystalline phase to the crystalline β-phase (CsCl type) after 20 h (planetary ball mill) or 30 h (vibrational ball mill). Generally, these differences are

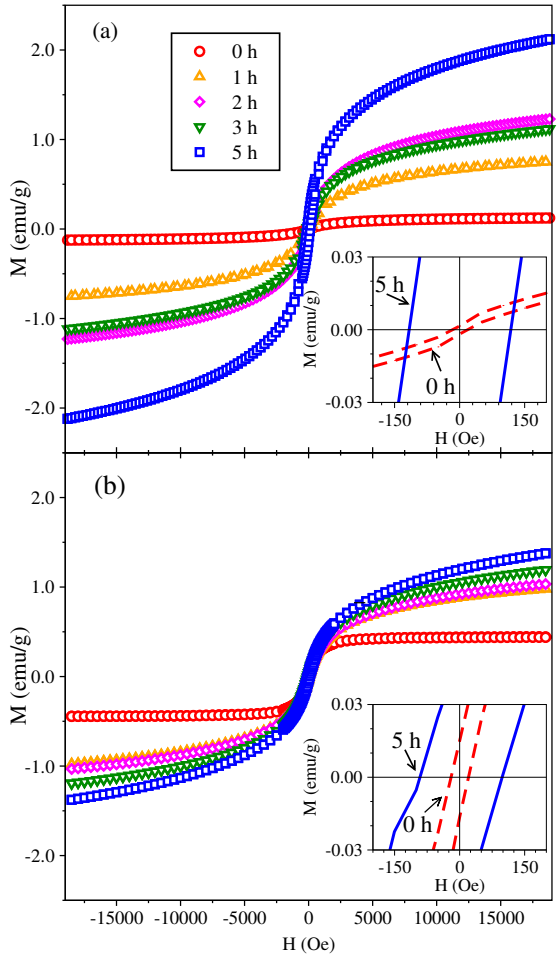

Fig. 4 Magnetization measurements at 300 K as a function of an applied field for the Al-Cu-Fe samples: (a) *i*-$Al_{64}Cu_{23}Fe_{13}$ and (b) ω-$Al_{70}Cu_{20}Fe_{10}$ alloys after different milling times. The insets show the part of the curves near to the origin for 0 and 5 hours milled samples.

attributed to the initial milling conditions[35].

The variations of the Mössbauer and magnetic parameters for un-milled and milled Al-Cu-Fe samples suggest that the chemical order, type of long range order, and the average grain size play an important role in the physical properties of Al-Cu-Fe systems. Thus, despite of having very close chemical compositions, the *i*-phase (with lattice parameter a=6.308(2) Å) and ω-phase (a=6.336(1) Å and c=14.870(2) Å) present a quite different long range order, as can be seen in Fig. 2 for the corresponding un-milled samples. Hence, we expect that their behavior during the mechanical milling process should be different. In fact, in Table 1 can be seen that the values of the hyperfine parameters for the un-milled samples (*i*-$Al_{64}Cu_{23}Fe_{13}$ and ω-$Al_{70}Cu_{20}Fe_{10}$) are completely different. In their corresponding Mössbauer spectra can be observed that the Fe site in the ω-phase have a more symmetric environment than in the quasicrystalline phase, which is expressed in their corresponding quadrupole splittings. In this regard, we can mention some important points considering a structural model for the 1/1 approximant of the Al-Cu-Fe phase (Cockayne model) employed to describe the icosahedral phase[36]. We note two Fe sites (Fe1 sites surrounded exclusively by aluminum atoms and Fe2 sites surrounded by Cu and predominantly by Al atoms), while in the ω-phase there is just one Fe site surrounded only by Al atoms. Therefore, it can be seen that these slight differences in the atomic local environment will play an important role in the nanostructuration process by mechanical milling, which is characterized by generating disordered sites in the interstitial region. Thus, it is expected that this might influence considerably in the physical properties of the studied samples. Also, the differences in the isomer shift values could be related to the amount of Fe atoms associated to each phase. According to this, the quasicrystalline phase with 13 at.% and the ω-phase with 10 at.% have $\langle\delta\rangle$=0.241 mm/s and 0.170 mm/s, respectively. These results are in agreement with Refs.[37] and[38]. However, the nanostructuration process does not affect significantly the isomer shift of the milled samples, as happened for M_s (see Table 1). This is expected because $\langle\delta\rangle$ is related to both the atomic radius and the electronic charge distribution in the nucleus, which remain almost constant during the MM process.

Furthermore, it is worth noting that the Mössbauer spectra during the nanostructuration process broadens. For the *i*-$Al_{64}Cu_{23}Fe_{13}$ samples, the Mössbauer spectra become wider, without changing their shape, after reducing the average grain size which is evidenced in the slight increment of the quadrupole splitting values (see Table 1). However, for the ω-$Al_{70}Cu_{20}Fe_{10}$ phase these variations are more pronounced. This remarkable difference could be explained considering the structural stability of the phases. It is known that the Bergman cluster is considered the building block of the icosahedral Al-Cu-Fe alloys (*i*-phase). This kind of atomic arrangement, consisting mainly of two atomic shells with icosahedral symmetry, is more stable than other kind of local order such as the tetragonal order observed in the ω-phase[39]. Additionally, according to the indicated above, the changes in the shape of the Mössbauer spectra (mainly in the ω-phase) means that the environment of some Fe sites are partially distorted. In fact, when the average grain size decreases, the shape of the quadrupole distribution, centered on $\langle\Delta\rangle$=0.415 mm/s, becomes slightly broader which is associated to the slight distortion of atomic environment in the icosahedral structure, as can be seen in the right panel of Fig. 2. The same behavior is observed in the ω-phase, but this distribution changes from a narrow peak (centered at $\langle\Delta\rangle$=0.152 mm/s) to a distribution with two peaks (centered at 0.168 mm/s and 0.587 mm/s). The second peak could be associated to small disorder in the grain boundary due to the employed technique for the nanostructuration process. In this sense, the same criterion is applied to the *i*-phase where such small quadrupole distribution peak would be overlapped by the full distribution curve (whose width is approximately the sum of the two peak widths in the ω-phase).

The M_s obtained for the 0 h quasicrystal (0.124 emu/g) is smaller than that reported by M. Roy (M_s=6.4 emu/g)[9]. This difference could be attributed to the presence of a remnant of the *bcc*-Fe phase in the samples synthesized in Ref.[9] because those samples were obtained by mechanical alloying of elemental powders of Al, Cu, Fe in the composition $Al_{65}Cu_{20}Fe_{15}$. In our case the QC sample is obtained by arc furnace and then mechanically milled to obtain the nanostructured QCs. Furthermore, the me-

chanical milling process contributes to a systematic increment of the magnetic parameters (M_s and H_c) for both compositions, as indicated before (see Table 1). This increment can be associated to the reduction of the average grain size or, in other words, to the growth of a magnetic interstitial region.

On the other hand, an important observation in these experiments is the absence of new phases during the nanostructuring process. Therefore, this ensures that the changes in the physical properties, in particular the magnetic ones, of the Al-Cu-Fe system should be related to the reduction of the average grain size of the system.

Hence, following Ref.[40] we estimate the magnetic fraction in the Al-Cu-Fe samples (i-$Al_{64}Cu_{23}Fe_{13}$ and ω-$Al_{70}Cu_{20}Fe_{10}$). For this purpose, we assume that the full magnetic moment of each iron atom is 2.2 μ_B. Then, if all the Fe ions were magnetic, the saturation magnetization should be $M_{s_i}=13\times2.2\mu_B$/f.u.=28.6 μ_B/f.u. for i-phase and $M_{s_\omega}=10\times2.2\mu_B$/f.u.= 22 μ_B/f.u. for ω-phase (f.u. standing for the "formula unit"). Now, knowing that for the un-milled i-phase the experimental value is $M_s^{exp}=0.124$ emu/g=0.087 μ_B/f.u. (see Table 1) we determine that only ~0.30% of all the Fe atoms in this sample carry a magnetic moment. Analogously, for the un-milled ω-phase we obtain that ~1.36% of the Fe atoms carry a magnetic moment. In similar way, we obtain the percentage of magnetic Fe atoms for the milled samples (nanostructured samples) and observe that these percentages increase after reducing the average grain size of the samples, as can be seen in Figs. 6(c) and 6(f). Thus, after five hours milling %Fe atoms with magnetic moments reaches ~4.89%, and ~4.85% for the i-phase and ω-phase, respectively. It is worth mentioning that a similar amount of magnetic atoms, for solid samples, have been reported in the Al-Cr-Fe approximant phase (0.8% of Fe atoms[40]) and the Al-Pd-Mn quasicrystal (1.0% of Mn atoms[30,41]).

However, according to Mössbauer spectroscopy measurements, no magnetic behavior is observed. In the other hand, the magnetization curves show a weak ferromagnetic behavior. This apparent disagreement between the VSM measurements, showing a magnetic behavior of the samples, and the Mössbauer spectra that do not show a magnetic signal (sextet lines) can be understood considering the following: (*i*) from XRD measurements there are no evidences of secondary phases, this implies that the observed magnetic signal cannot be due to the formation of spurious phases during the MM process; (*ii*) it is known that VSM is much more sensitive to detect a magnetic signal than TMS; consequently, can be argued that the percentage of magnetic Fe sites is below the detection limit of TMS, as was observed in several systems[42,43]. To test this idea, we mixed *bcc*-Fe with the QC so that the amount of the Fe sites in the *bcc*-Fe phase represents ~1.9% of the total amount of Fe (*bcc*-Fe and QC together). As suggested, the resulting spectrum did not show any magnetic signal with TMS (sextet lines). We also carried out a chemical analysis by energy dispersive X-ray spectroscopy (EDX) of the samples. The results indicate a low presence of chromium for the five hours milled samples (of the order of 0.25 Wt.% and 0.16 Wt.% for the i-phase and the ω-phase, respectively), which is due to contamination by the milling tools (hardened steel vial and balls). Thus, one could argues that the magnetic signal is due to Cr. However, Cr is not found in the samples milled by 0.5 hours. Contrary, their corresponding M_s values increase from 0.124 emu/g to 0.784 emu/g (6 times higher) in the i-phase and from 0.449 emu/g to 0.854 emu/g (2 times higher) in the ω-phase. Thus, the variation of M_s cannot be attributed to Cr. In general, Cr is present during the full milling process but its variation is not in the same proportion as the variations of M_s, as indicated above (see Table 1). Analogously, oxygen is also present during the milling process. However, for 0.5 hours milling the increment of O is of ~1.9 while M_s increases 6 times (i-phase). Hence, the presence of oxygen could be associated to a very thin aluminum oxide layer[44] without magnetic signal. In summary, we do not neglect the possibility that impurities, originated from the milling tool debris (formation of iron oxides or external elements like Cr), could contribute to the observed magnetism. However, the noticeable difference in the variation of the magnetic response for both milled samples (16 and 3.5 times higher than its corresponding solid counterpart for i-phase and ω-phase, respectively) is a clear indication that the magnetic signal is not only due to the employed experimental procedure, which is of the same type and order in both samples, but mainly due to a physical origin. In this regard, Jagličić *et al.* presented a study of the Mn magnetism in the i-Al-Pd-Mn quasicrystal subjected to different thermal annealing sequences. They reported that the degree of the disorder induced in the i-Al-Pd-Mn quasicrystalline structure, during the heat treatments or cooling modes, was decisive to generate the magnetic moment formation in this sample[45]. In similar way, we consider that in the case of the milled Al-Cu-Fe samples, the impact of the balls produces lattice defects and grain boundaries in the system. For longer milling times the grain border becomes an interstitial disordered region that grows after increasing the milling of the samples. This disorder could be correlated with the observed magnetic response. However, since the i-$Al_{64}Cu_{23}Fe_{13}$ phase is generally not perfect in the structure (which can contain twin domains or nucleation of approximants locally) the origin of the magnetic properties may be more complex than only disorder. Further measurements on atomic scale are required to understanding and clarify this magnetic behavior, which is beyond the scope of this study.

4.1 Dependence of the physical properties with the grain size

The systematic variation of the structural and magnetic parameters during the nanostructuration process makes us wonder if these physical properties scale with system size. In this sense, to study the dependence of these parameters as function of the average grain size we use the scaling theory[46], which in its simplest form means that we can express this dependence as a power law function of the form $F = F_o + b\langle D\rangle^{\alpha}$. The parameter F is related to the physical quantities ($\langle\delta\rangle$, $\langle\Delta\rangle$, M_s and H_c in our case), and α is called the scaling parameter. F_o and b are constants such that F_o represents the value of F in the bulk case. Thus, in the macroscopic limit the last expression should satisfy $F \to F_o$ when $\langle D\rangle \to \infty$; hence, $\alpha < 0$. However, according to the average grain size values obtained for the 0 h milling Al-Cu-Fe alloys (of the

order of 100 nm, see Fig. 3), our samples are far away from the ideal solid sample. Then, the expression above can be reduced to the form

$$F = b\langle D\rangle^{\alpha}, \quad (2)$$

so that eq. (2) will only be applied in the range of the experimental values of $\langle D\rangle$ (nanometer order). Furthermore, according to the scaling theory the highlight of this equation is the value of α for each system. For this reason, we present a log-log plot (base 10) of F. The experimental data (obtained from Table 1) show the expected linear increase of F after reducing the average grain size, as shown in Figs. 5 and 6. It is evident that there is not a transition in the studied region. This might indicate that under the milling conditions employed, the samples have not reached a critical grain size, where considerable changes of the physical properties are expected; i.e., a change of the value of α in the fit. The α values obtained from the slope of the curves are summarized in Table 2. The meaning of α from Table 2 could be interpreted as the speed of the variation of the physical quantities with the average grain size. For instance, the α values of $\langle\delta\rangle$ and $\langle\Delta\rangle$ for the i-$Al_{64}Cu_{23}Fe_{13}$ are low compared to the ω-phase, which is in agreement to the high structural stability of the icosahedral system. The same occur for H_c. However, M_s changes faster in the i-phase than in the ω-phase.

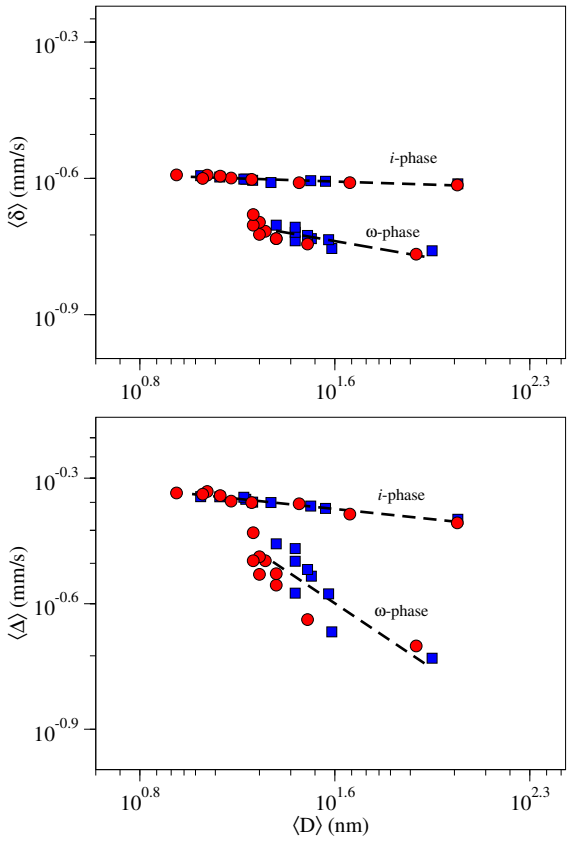

Fig. 5 Variation of hyperfine parameters, $\langle\delta\rangle$ and $\langle\Delta\rangle$, versus the average grain size $\langle D\rangle$ plotted on a log-log scale (○ series A, □ series B). The dashed lines indicate a fit according to equation (2). From the slope of the fit we obtain the exponent α. The error bars are smaller than or equal to the symbol sizes.

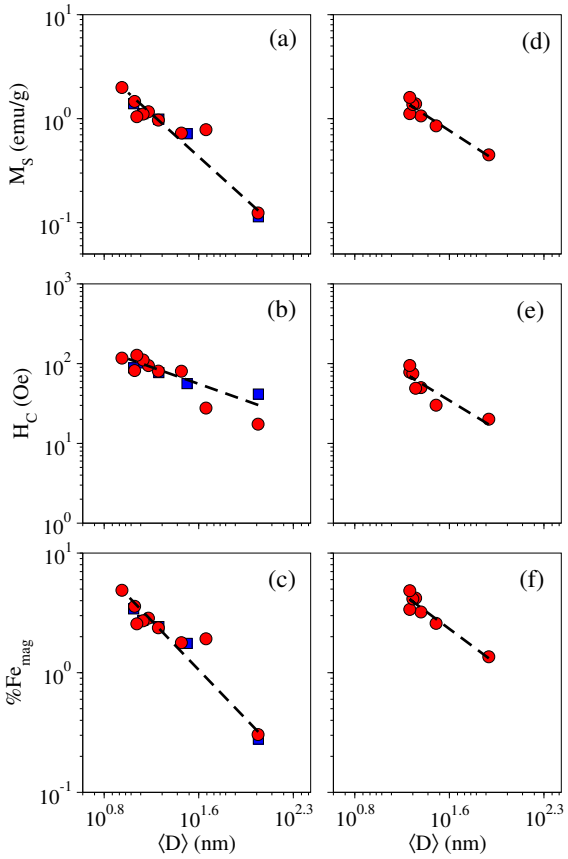

Fig. 6 Log-log plot of the variation of the saturation magnetization (M_s), coercivity (H_c) and %Fe atoms carry magnetic moment with the average grain size $\langle D\rangle$ for (a)-(c) quasicrystalline i-$Al_{64}Cu_{23}Fe_{13}$ and (d)-(f) crystalline ω-$Al_{70}Cu_{20}Fe_{10}$ samples (○ series A, □ series B). The dashed lines indicate a fit according to equation (2). From the slope of the fit we obtain the exponent α. The error bars are smaller than symbol size.

The difference in these changes is associated to the larger content of Fe atoms and the smaller average grain size (13 at.%Fe, ~9 nm) in the i-phase, as compared to the ω-phase (10 at.%Fe, ~19 nm). Furthermore, the slight difference of the exponent α, corresponding to M_s (see Table 2), should be related to the type of long range order.

Table 2 The α values for the hyperfine and magnetic parameters of both compositions: i-$Al_{64}Cu_{23}Fe_{13}$ quasicrystalline and ω-$Al_{70}Cu_{20}Fe_{10}$ crystalline phases

	α	
F	i-phase	ω-phase
$\langle\delta\rangle$	-0.018	-0.096
$\langle\Delta\rangle$	-0.063	-0.402
M_s	-1.059	-0.757
H_c	-0.540	-0.926

5 Conclusions

In conclusion, we observe an increment of the ferromagnetic behavior during the mechanical milling of both Al-Cu-Fe samples. The initial saturation magnetization of the *i*-$Al_{64}Cu_{23}Fe_{13}$ and the ω-$Al_{70}Cu_{20}Fe_{10}$ is 0.124 emu/g and 0.449 emu/g, respectively. These small values indicate that only 0.30% for the *i*-phase and 1.36% for the ω-phase of the Fe atoms carry magnetic moment. As a result of the mechanical milling process, the magnetic response of the ω-phase increases up to 3.5 times higher than its corresponding solid counterpart. Surprisingly, for the case of the *i*-phase this increment is around 16 times. From XRD analysis we found that the nanostructured *i*-phase have an average grain size of 9 nm while the ω-phase, 19 nm.

Considering that the interstitial region depends inversely of the volume ($\sim\langle D\rangle^{-3}$) of the nano-grains, we can express (according to the scaling theory) the dependence of the magnetic response with the average grain size as a power law function where the exponent α is the relevant quantity. In this way, we can determine the speed of the variation of the studied physical parameters after reducing the average grain size during the nanostructuration process. Thus, the values of α, corresponding to the magnetic response, are slightly different in each phase, which could be related to the different chemical composition and/or the type of long range order. Additionally, we also search for a critical grain size. However, this critical value has not been observed in the studied samples.

It is worth mentioning that a similar behavior in terms of grain size reduction has also been found in other alloys. Hence, the study of the parameter α is required to explore its possible universal behavior as well as to find a critical grain size in the nanostructured samples. In particular, Al-rich based alloys offers interesting perspectives due to their similarities to the Al-Cu-Fe system. Furthermore, similar studies in other quasicrystals with greater magnetism (such as Al-Pd-Mn or Al-Cu-Co) could be interesting to find if its magnetic response increases in the same proportion as in the case of the *i*-$Al_{64}Cu_{23}Fe_{13}$. Finally, it is necessary to have a clear understanding of the magnetic behavior of both Al-Cu-Fe phases during the mechanical milling process. Thus, further HRTEM or STEM images at atomic resolutions are required. Additional studies to quantify and/or discard completely the possible contamination of the milling tool debris are being planned. Hence, a study of the nanostructuration of the samples employing other type of containers (e.g. agate and/or zirconia tools), which do not contain magnetic elements, is also required.

Acknowledgments

The authors would like to thank J. Dolinšek for helpful discussions of the results of this work. M. Pillaca and M. Z. Pinto acknowledge the "Zuñiga and Rivero Family Association" for financial support under its fellowship program for master studies at the San Marcos University. This research was funded by CSI-VRI-UNMSM under Project N° 131301011.

References

1 J. M. Dolinšek, Chem. Soc. Rev., 2012, **41**, 6730–6744.
2 A. P. Tsai, Chem. Soc. Rev., 2013, **42**, 5352–5365.
3 J. M. Dubois, Mater. Sci. Eng. A, 2000, **294-296**, 4–9.
4 D. Shechtman, I. Blech, D. Gratias and J. W. Cahn, Phys. Rev. Lett., 1984, **53**, 1951–1953.
5 M. Bobnar, P. Jeglič, M. Klanjšek, Z. Jagličić, M. Wencka, P. Popčević, J. Ivkov, D. Stanić, A. Smontara, P. Gille and J. Dolinšek, Phys. Rev. B, 2012, **85**, 024205.
6 J. Dolinšek, P. Jeglič, P. J. McGuiness, Z. Jagličić, A. Bilušić, Ž. Bihar, A. Smontara, C. V. Landauro, M. Feuerbacher, B. Grushko and K. Urban, Phys. Rev. B, 2005, **72**, 064208.
7 A. A. Rempel, S. Z. Nazarova and A. I. Gusev, J. Exp. Theor. Phys. Lett., 2000, **72**, 144–147.
8 Z. M. Stadnik, G. Stroink, H. Ma and G. Williams, Phys. Rev. B, 1989, **39**, 9797–9805.
9 M. Roy, J. Magn. Magn. Mater., 2006, **302**, 52–55.
10 Y. Hattori, K. Fukamichi, K. Suzuki, A. Niikura, A. P. Tsai, A. Inoue and T. Masumoto, J. Phys.: Condens. Matter, 1995, **7**, 4183–4191.
11 A. I. Goldman, T. Kong, A. Kreyssig, A. Jesche, M. Ramazanoglu, K. W. Dennis, B. S. L. and P. C. Canfield, Nature Mater., 2013, **12**, 714–718.
12 Z. M. Stadnik, in Physical Properties of Quasicrystals, Springer-Verlag, Berlin Heidelberg, 1999, p. 295.
13 A. P. Tsai, A. Inoue and T. Masumoto, Jpn. J. Appl. Phys., 1987, **26**, L1505–L1507.
14 J. Dolinšek, S. Vrtnik, M. Klanjšek, Z. Jagličić, A. Smontara, I. Smiljanić, A. Bilušić, Y. Yokoyama, A. Inoue and C. V. Landauro, Phys. Rev. B, 2007, **76**, 054201.
15 P. Baláž, Mechanochemistry in Nanoscience and Minerals Engineering, Springer-Verlag, Heidelberg, 2008.
16 C. Suryanarayana, Mechanical Alloying and Milling, Marcel Dekker, New York, 2004.
17 J. J. Torres-Vega, L. R. Medrano, C. V. Landauro and J. Rojas-Tapia, Physica B, 2014, **436**, 74–79.
18 M. Z. Pinto, M. Pillaca, C. V. Landauro, J. Quispe-Marcatoma, C. Rojas-Ayala, V. A. Peña Rodriguez and B. E., Hyperfine Interact., 2014, **224**, 83–88.
19 J. Quispe Marcatoma, C. V. Landauro, M. Taquire, C. Rojas Ayala, M. Yaro and V. A. Peña Rodriguez, Hyperfine Interact., 2010, **195**, 105–109.
20 J. Quispe-Marcatoma, C. Rojas-Ayala, C. V. Landauro, M. A. de Souza, F. Pelegrini, M. Taquire, V. A. Peña Rodriguez and E. Baggio-Saitovitch, Hyperfine Interact., 2011, **203**, 1–8.
21 R. A. Brand, Normos Mössbauer Fitting Program, User's Guide, Univ. Duisburg, Germany, 1995.
22 J. W. Cahn, D. Shechtman and D. Gratias, J. Mat. Sci., 1986, **1**, 13–26.
23 M. Cornier-Quiquandon, A. Quivy, S. Lefebvre, E. Elkaim, G. Heger, A. Katz and D. Gratias, Phys. Rev. B, 1991, **44**, 2071–2084.
24 P. Weisbecker, G. Bonhomme, G. Bott and J. M. Dubois, J. Non-Cryst. Solids, 2005, **351**, 1630–1638.
25 G. Laplanche, A. Joulain, J. Bonneville, V. Gauthier-Brunet and S. Dubois, Mater. Sci. Eng. A, 2010, **527**, 4515–4518.

26 S. D. Kaloshkin, V. V. Tcherdyntsev and A. I. Laptev, 2004, **39**, 5399–5402.

27 B. D. Cullity, Elements of X-ray Diffraction, Addison-Wesley, Massachusetts, 1978, p. 284.

28 S. Li, K. Wang, L. Sun and Z. Wang, Scr. Metall. Mater., 1992, **27**, 437–442.

29 Z. M. Stadnik and G. Stroink, Phys. Rev., 1988, **38**, 447–453.

30 M. A. Chernikov, A. Bernasconi, C. Beeli, A. Schilling and H. R. Ott, Phys. Rev. B, 1993, **48**, 3058–3065.

31 J. Barzola-Quiquia, A. Lessig, A. Ballestar, C. Zandalazini, G. Bridoux, F. Bern and P. Esquinazi, J. Phys.: Condens. Matter, 2012, **24**, 1–12.

32 M. Pillaca and C. V. Landauro, Revista de Investigación de Física, 2012, **15**, 121501102.

33 N. K. Mukhopadhyay and T. P. Yadav, Isr. J. Chem., 2011, **51**, 1185–1196.

34 C. Patiño-Carachure, O. Téllez-Vázquez and G. Rosas, J. Alloys Compd., 2011, **509**, 10036–10039.

35 C. C. Koch, Nanoestructured materials: Processing, properties and applications, William Andrew, New York, 2nd edn, 2007, p. 730.

36 E. S. Zijlstra, J. Kortus, M. Krajčí, Z. M. Stadnik and S. K. Bose, Phys. Rev. B, 2004, **69**, 094206.

37 V. Srinivas and R. A. Dunlap, Philos. Mag. B, 1991, **64**, 475–484.

38 N. Kataoka, A. P. Tsai, A. Inoue, T. Masumoto and Y. Nakamura, Jpn. J. Appl. Phys., 1988, **27**, L1125–L1127.

39 M. G. Bown and P. J. Brown, Acta Crystallogr., 1956, **9**, 911–915.

40 Ž. Bihar, A. Bilušić, J. Lukatela, A. Smontara, P. Jeglič, P. J. McGuiness, J. Dolinšek, Z. Jagličić, J. Janovec, V. Demange and J. M. Dubois, J. Alloys Compd., 2006, **407**, 65–73.

41 J. Dolinšek, M. Klanjšek, Z. Jagličić, A. Bilušić, Z. and A. Smontara, J. Phys.: Condens. Matter, 2002, **14**, 6975–6988.

42 K. Nomura, C. A. Barrero, K. Kuwano, Y. Yamada, T. Saito and E. Kuzmann, Hyperfine Interact., 2009, **191**, 25–32.

43 C. Gao, F. Lin, X. Zhou, W. Shi and A. Liu, J. Alloys Compd., 2013, **565**, 154–158.

44 C. Zhou, H. Xu, S. Gong and G. Kang, J. Mater. Sci. Technol., 2002, **18**, 251–253.

45 Z. Jagličić, M. Jagodič, B. Grushko, E. S. Zijlstra, T. Weber, W. Steurer and J. Dolinšĕk, Intermetallics, 2010, **18**, 623–632.

46 M. Schreiber, J. Phys. C: Solid State Phys., 1985, **18**, 2493–2505.